

การจำลองผลของสนามไฟฟ้าต่อสมบัติโพลาริเซชันของแสงที่เปล่งจากควอนตัมดอท

ชนิดอินเดียมอาร์เซไนด์ที่เรียงกันแบบประกอบขึ้นเอง



นาย ชลกร เชี่ยวพานิช

วิทยานิพนธ์นี้เป็นส่วนหนึ่งของการศึกษาตามหลักสูตรปริญญาวิศวกรรมศาสตรมหาบัณฑิต

สาขาวิชาวิศวกรรมไฟฟ้า ภาควิชาวิศวกรรมไฟฟ้า

คณะวิศวกรรมศาสตร์ จุฬาลงกรณ์มหาวิทยาลัย

ปีการศึกษา 2553

ลิขสิทธิ์ของจุฬาลงกรณ์มหาวิทยาลัย



**SIMULATION OF ELECTRIC-FIELD EFFECT ON THE OPTICAL POLARIZATION PROPERTY
OF SELF-ASSEMBLED INDIUM-ARSENIDE ALIGNED QUANTUM DOTS**

Mr. Chonlakorn Chiewpanich

**A Thesis Submitted in Partial Fulfillment of the Requirements
for the Degree of Master of Engineering Program in Electrical Engineering**

Department of Electrical Engineering

Faculty of Engineering

Chulalongkorn University

Academic Year 2010

Copyright of Chulalongkorn University

532375

Thesis Title SIMULATION OF ELECTRIC-FIELD EFFECT ON THE OPTICAL
POLARIZATION PROPERTY OF SELF-ASSEMBLED INDIUM-
ARSENIDE ALIGNED QUANTUM DOTS


By Mr. Chonlakorn Chiewpanich

Field of Study Electrical Engineering

Thesis Advisor Chanin Wissawinthanon, Ph.D.

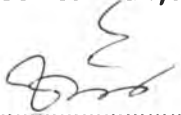
Thesis Co-Advisor Professor Somchai Ratanathammaphan, D.Eng.

Accepted by the Faculty of Engineering, Chulalongkorn University in Partial
Fulfillment of the Requirements for the Master's Degree


..... Dean of the Faculty of Engineering
(Associate Professor Boonsom Lerthirunwong, Dr.Ing.)


THESIS COMMITTEE


..... Chairman
(Professor Somsak Panyakeow, D.Eng.)


..... Thesis Advisor
(Chanin Wissawinthanon, Ph.D.)

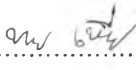

..... Thesis Co-Advisor
(Associate Professor Somchai Ratanathammaphan, D.Eng.)



..... Examiner
(Associate Professor Banyong Toprasertpong, Dr.Ing.)



..... External Examiner
(Noppadon Nuntawong, Ph.D.)

ชลกร เชี่ยวพานิช : การจำลองผลของสนามไฟฟ้าต่อสมบัติโพลาริเซชันของแสงที่เปล่งจากควอนตัมดอตอินเดียมอาร์เซไนด์ที่เรียงกันแบบประกอบขึ้นเอง. (SIMULATION OF ELECTRIC-FIELD EFFECT ON THE OPTICAL POLARIZATION PROPERTY OF SELF-ASSEMBLED INDIUM-ARSENIDE ALIGNED QUANTUM DOTS) อ. ที่ปรึกษาวิทยานิพนธ์หลัก: อ. ดร.ชรินทร์ วิศวินชานนท์, อ. ที่ปรึกษาวิทยานิพนธ์ร่วม: รศ. ดร.สมชัย รัตนธรรมพันธ์, 311 หน้า.

วิทยานิพนธ์ฉบับนี้ได้จำลองระบบสนามไฟฟ้าในสองมิติเพื่อนำไปใช้กับแบบจำลองจุดควอนตัมอินเดียมอาร์เซไนด์ที่เรียงกันแบบประกอบขึ้นเอง เพื่อวิเคราะห์สมบัติโพลาริเซชันเชิงแสง โดยใช้ระเบียบวิธีทางไฟไนต์ดิฟเฟอเรนซ์ในการแก้ปัญหา ซึ่งสอดคล้องกับจำนวนจุดตารางในฐานะที่เป็นตัวกำหนดความแม่นยำสำหรับการคำนวณ จากการศึกษาพบว่าระดับชั้นโพลาริเซชันเชิงเส้น (degree of linear polarization) ภายใต้อิทธิพลของสนามไฟฟ้าที่ใส่เข้ามาขึ้นอยู่กับปัจจัยหลัก ดังนี้ จำนวนของจุดควอนตัม ความแรงของสนามไฟฟ้า ระยะห่างระหว่างจุดควอนตัมที่ติดกัน และขนาดของจุดควอนตัม ทิศของสนามไฟฟ้าในแนวขนานกับการเรียงตัวของจุดควอนตัมมีผลกระทบต่อระดับชั้นโพลาริเซชันมากกว่าในทิศของสนามไฟฟ้าที่ตั้งฉากกับการเรียงตัวของจุดควอนตัม โครงสร้างจุดควอนตัมที่เรียงตัวกันจะมีระดับชั้นโพลาริเซชันสูงขึ้นขณะที่ความแรงของสนามไฟฟ้าเพิ่มขึ้น แต่จะมีค่าลดลงได้เมื่อสนามไฟฟ้าที่มีค่าแรงมากเกินไป จำนวนของจุดควอนตัมที่เพิ่มขึ้นจะส่งผลให้ระดับชั้นโพลาริเซชันมีค่าสูงขึ้น แต่ในที่สุดอาจนำไปสู่การลดลงของแรงดันไฟฟ้าที่ก่อให้เกิดระดับชั้นโพลาริเซชันค่าสูงสุด นอกจากนี้จุดควอนตัมที่อยู่ใกล้กันมากขึ้นก็สามารถส่งผลให้ระดับชั้นโพลาริเซชันสูงขึ้นด้วย อย่างไรก็ตาม ขนาดของจุดควอนตัมที่ใหญ่ขึ้นกลับทำให้ระดับชั้นโพลาริเซชันมีค่าลดลง จากการวิเคราะห์ผลการทดลองเหล่านี้พบว่า หากจุดควอนตัมอยู่ใกล้กันมากขึ้น จุดควอนตัมมีขนาดเล็กลง จุดควอนตัมเรียงกันเป็นจำนวนมากขึ้น และ/หรือ ภายใต้อิทธิพลของสนามไฟฟ้าที่มีขนาดเหมาะสม จะส่งผลให้ระดับชั้นโพลาริเซชันเชิงเส้นยังมีค่าเพิ่มขึ้น การสังเคราะห์ผลการทดลองที่กล่าวมาแล้วทั้งหมดนี้ทำให้เรามีความรู้ความเข้าใจในแง่ของฟิสิกส์จากสมบัติดังกล่าวมากขึ้น ทั้งเป็นการเปิดโลกทัศน์ทางด้านความคิดในเชิงมุมมองที่กว้างขึ้นอีกด้ว องค์ความรู้ดังกล่าวสามารถที่จะนำไปสู่การพัฒนาสิ่งประดิษฐ์สารกึ่งตัวนำทางแสงที่มีประสิทธิภาพสูงในระยะเวลาอันใกล้

ภาควิชา วิศวกรรมไฟฟ้าลายมือชื่อนิสิต 

สาขาวิชา วิศวกรรมไฟฟ้าลายมือชื่อ.ที่ปรึกษาวิทยานิพนธ์หลัก 

ปีการศึกษา 2553ลายมือชื่อ.ที่ปรึกษาวิทยานิพนธ์ร่วม 

5070548521 : MAJOR ELECTRICAL ENGINEERING

KEYWORDS: ALIGNED QUANTUM DOTS/ POLARIZATION DEGREE / ELECTRIC FIELD

CHONLAKORN CHIEWPANICH: SIMULATION OF ELECTRIC-FIELD EFFECT ON THE OPTICAL POLARIZATION PROPERTY OF SELF-ASSEMBLED INDIUM-ARSENIDE ALIGNED QUANTUM DOTS. THESIS ADVISOR: CHANIN WISSAWINTHANON, Ph.D., THESIS CO-ADVISOR: ASSOC. PROF. SOMCHAI RATANATHAMMAPHAN, D.Eng., 311 pp.

The simulation of two-dimensional externally applied electric field system was introduced to implement with self-assembled InAs aligned quantum dots (QDs) in order to investigate the optical polarization property of those QDs. The methodology was based on the numerical finite-difference (FDM) method related to number of grid points, which determines the accuracy of the calculation. From the study, it was found that the linear polarization degree (PD) of the aligned QDs under applied electric field significantly depends on number of QDs in the system, the field strength, the interdot spacing, and the size of the QDs. The electric field applied parallel to the alignment of QDs has stronger effect on the degree of optical polarization than that applied in the direction perpendicular to alignment. The aligned QDs manifest good response with an increase of applied field by a larger polarization anisotropy, but turns to decrease in circumstance of strong field. A higher PD value from higher number of QDs was observed and eventually lead to a shift of applied voltage to lower potential, corresponding to maximum PD value. Moreover, very close separation between adjacent QDs also produces a strong polarization. By contrast, the calculation shows a reduction of PD value as enlargement of QDs. From these results, it may be concluded that closer spacing, smaller dot size, more number of QDs in the alignment, and/or suitable magnitude of applied electric field gives rise to a higher polarization degree of aligned QDs structure. The synthesis of results connected to the physics behind them render better understanding and broaden the horizon in the intellectual aspect of thought process, as well. This interesting knowledge would lead to a development in high-efficiency semiconductor optoelectronic devices in the short run.

Department: Electrical Engineering Student's Signature 

Field of Study: Electrical Engineering Advisor's Signature 

Academic Year: 2010 Co-Advisor's Signature 

Acknowledgements

First, I would like to be greatly thankful to my advisor, Dr. Chanin Wissawinthanon, my thesis co-advisor Dr. Somchai Ratanathamphan, and head of the SDRL Laboratory Professor Dr. Somsak Panyakeow, for the topic of this thesis work, straightforward advice, taking care of my life in the laboratory, fine correction my work, especially answering my questions, not only describing thoroughly with attaching the other gainful knowledge, but also posing a question back to me, which sets an example of creativity and broadening horizon in the intellectual aspect of thought process. They activated me to work hard to produce a high standard of the thesis work, which is probably the most important thing I could have ever learned.

I am very grateful to acknowledge other committee members of my thesis defense Dr. Banyong Toprasertpong and Dr. Noppadon Nuntawong (the external committee member from National Electronics and Computer Technology Center of Thailand) for evaluating my work with quality, and my others teachers from SDRL for transferring useful knowledge to me.

Many thanks go to my special friends: Wichit Tantiweerasophon, Matinon Maitreeborirak, and Samatcha Vorathamrong, for their invaluable assistance of everything and our friendship forever. My colleagues behave like my brotherhoods and give me the notable memorials throughout a period of my Master's Degree education. Particularly, I am remarkably indebted for three persons: Nattajak Siribanluoewut, Nirat Patanasemakul, and Wasinee Kheansaard (the last person helped me to support the additional papers that cannot be downloaded from Chulalongkorn University). Without their guidance and mentorship, this thesis would not certainly have been successful. My special thanks distribute to my family for their love and encouragement, all of my life.

I would like to acknowledge the Asian Office of Aerospace Research and Development (AOARD), Office of the High Education Commission, Thailand Research Fund (TRF), Nanotechnology Center of Thailand (Nanotech), and Chulalongkorn University, for their financial support and cooperation.

Finally, I would like to say "thank you" myself for my deep spirit that leads to manifest my absolute potential to face all the obstacles during working on this thesis. My gladness is also devoted to John McLaughlin: my idol, all the time.

CONTENTS

| | Page |
|--|-----------|
| Abstract (Thai) | iv |
| Abstract (English) | v |
| Acknowledgements | vi |
| Contents | vii |
| List of Tables | xi |
| List of Figures | xii |
| | |
| Chapter I : Introduction | 1 |
| 1.1 Background | 1 |
| 1.2 Self-Assembled Aligned Quantum Dots | 4 |
| 1.3 Effect of Electric Field | 5 |
| 1.4 Objectives | 6 |
| 1.5 Scope of Work | 7 |
| 1.6 Research Methodology | 8 |
| 1.7 Significance of the Research | 9 |
| 1.8 Overview | 9 |
| | |
| Chapter II : Low-Dimensional Semiconductor Nanostructures: Quantum Confinement and Its Effect on Optical Properties | 11 |
| 2.1 Basic Concepts of Low-Dimensional Nanostructures | 11 |
| 2.1.1 Carrier Confinement and Energy Level Quantization | 13 |
| 2.1.2 Bulk Material | 17 |
| 2.1.3 Quantum Wells | 18 |
| 2.1.4 Quantum Wires | 19 |
| 2.1.5 Quantum Dots | 20 |
| 2.2 Quantum Confinement Effects on Optical Properties of Semi- conductor Nanostructures | 23 |
| 2.2.1 Optical Properties With Size Dependence | 25 |

| | Page |
|--|------|
| 2.2.2 Increase of Oscillator Strength | 25 |
| 2.2.3 New Intraband Transition..... | 26 |
| 2.2.4 Increased Exciton Binding Energy..... | 27 |
| 2.2.5 Dielectric Confinement Effect..... | 28 |
| 2.2.6 Increase of Transition Probability in Indirect-Bandgap Semiconductors..... | 28 |
| 2.2.7 Nonlinear Optical Properties Caused by the Quantum Confinement Effect..... | 29 |
| 2.3 Quantum Dots : Fundamentals, Physics, and Quantum Theore- tical Concepts..... | 31 |
| 2.3.1 Energy Levels..... | 31 |
| 2.3.2 Size Quantization in Quantum Dots | 34 |
| 2.3.3 Spontaneous Emission of Quantum Dots..... | 40 |
| 2.3.3.1 The physical system | 43 |
| 2.3.3.2 The luminescence equations | 47 |
| 2.3.3.3 The QD photoluminescence intensity | 48 |
| 2.4 Growth of The Quantum Dot | 51 |
| 2.4.1 Molecular Beam Epitaxy (MBE)..... | 51 |
| 2.4.2 Self-Assembled Growth Modes | 55 |
| 2.4.3 Self-Assembled Aligned QDs | 58 |
| 2.5 Effect of The Electric Field on Nanostructures | 61 |
| 2.5.1 Electric Field on Bulk Structure: The Franz-Keldysh Effect | 62 |
| 2.5.2 Electric Field on Quantum Well Structure : The Quantum Confined Stark Effect (QCSE)..... | 69 |
| 2.5.3 Electric Field on Quantum Dot Structure | 79 |
| 2.5.3.1 Theoretical concept of electric field on semiconductor quantum dot | 80 |
| 2.5.3.2 Theoretical studies of vertical and parallel electric field on semiconductor quantum dot..... | 91 |

| | Page |
|---|------------|
| 2.5.3.3 Experimental investigation of electric field on quantum dot structure | 95 |
| 2.6 Polarization Studies of The Quantum Dot..... | 101 |
| 2.6.1 Polarization Anisotropy in Quantum Dot Structure | 102 |
| 2.6.2 Effect of Electric Field on the Polarization in Quantum Dots | 111 |
| Chapter III : Calculation Details..... | 122 |
| 3.1 Simulation of the Self-Assembled Aligned Quantum Dots..... | 122 |
| 3.1.1 Mathematical Model | 122 |
| 3.1.2 Theory | 124 |
| 3.1.3 Numerical Calculation in Two Dimensional Rectangular Aligned QDs | 125 |
| 3.1.4 Results and Discussion | 129 |
| 3.1.4.1 Comparison and verification the results calculated between two programs | 129 |
| 3.1.4.2 Coupling effect on the linear optical polarization property | 135 |
| 3.1.4.2.1 Single quantum dots | 136 |
| 3.1.4.2.2 Aligned quantum dots | 141 |
| 3.2 Calculation of Two-Dimensional Electric Field System | 151 |
| 3.2.1 Mathematical Model | 152 |
| 3.2.2 Simulation of Two-Dimensional Electric Field System by Numerical Approach | 153 |
| 3.2.3 Results and Discussion | 167 |
| 3.3 Conclusion..... | 179 |

| | Page |
|---|---------|
| Chapter IV : Results & Discussion | 181 |
| 4.1 Quantum Dots in Two-Dimensional Electric Field System | 181 |
| 4.1.1 Influence of the Electric Field Direction on Polarization Degree | 184 |
| 4.2 LPD Characteristic of Single QD under the Electric Field | 191 |
| 4.2.1 Increase of Polarization Degree of Isotropic QD with Applied Electric Field..... | 191 |
| 4.2.2 Optical Polarization Characteristic on Elongated QD Structure under Electric Field along the Direction of Elongation..... | 194 |
| 4.2.3 Comparison of Polarization Degree on Various QD Aspect Ratios in the Environment of Applied Electric Field..... | 196 |
| 4.3 LPD Characteristic of Aligned QDs under the Electric Field..... | 206 |
| 4.3.1 Effects of Electric Field Strength on the Polarization Degree | 206 |
| 4.3.2 Variation of Polarization Degree with Interdot Spacing under Electric Field..... | 219 |
| 4.3.3 Comparison of Polarization Degree for Various QD Sizes in Presence of Electric Field..... | 228 |
| 4.3 Overall Discussion | 239 |
| Chapter V : Conclusions | 244 |
| References | 249 |
| Appendices | 269 |
| Appendix A: Matlab® Program | 270 |
| Appendix B: List of Publications | 286 |
| Vitae | 287 |

LIST OF TABLES

| | | Page |
|-----------|---|------|
| Table 3.1 | Comparison of the modeling of QD structure for three different dimensions | 125 |
| Table 3.2 | The effective electron and heavy hole mass parameters (m_e is electron mass)..... | 130 |
| Table 3.3 | Comparison of ground-state eigen energy of four coupled QDs calculated by Matlab® programming and COMSOL Multiphysics | 134 |
| Table 3.4 | Comparison of polarization degree of QDs with various sizes and aspect ratios | 140 |
| Table 4.1 | Comparison of PD values with various sizes, aspect ratios, and applied voltages | 203 |
| Table 4.2 | The polarization degree vs. applied voltage of twelve QDs | 214 |
| Table 4.3 | The $V_{PD(max)}$ vs. QDs sizes & number of QDs at interdot spacing of 2 and 6 nm | 233 |

LIST OF FIGURES

| | | Page |
|-------------|--|------|
| Figure 2.1 | Schematic comparison of bulk semiconductor, waveguide for visible light, QD, and atom | 14 |
| Figure 2.2 | Comparison of electronic levels and spectral properties in atoms, bulk semiconductors and QDs | 14 |
| Figure 2.3 | Schematic views and graphs of (a) bulk, (b) quantum wells, (c) quantum wires, and (d) QD and their density of states (D.O.S.). L is in macroscopic scale (\sim cm), while L_x, L_y, L_z are in nanoscale..... | 15 |
| Figure 2.4 | Schematic representation of the lowest three level of carrier's energy quantization in potential well with the width of L_z (comparable to de Broglie wavelength). The picture shows examples of the three lowest-energy standing waves which can be happened in potential well (solid line) and the corresponding carrier's energy level of the de Broglie wavelength from the standing wave (dotted line), i.e. $E_1, E_2,$ and E_3 . The energy of each level is given by $E_{n,z} = \hbar^2 (n\pi)^2 / 2m^* L_z^2$, where n is a integer number of the level..... | 16 |
| Figure 2.5 | Evolution of the threshold current of semiconductor lasers..... | 22 |
| Figure 2.6 | Tree diagram of optical transition of quantum-confined semiconductors | 23 |
| Figure 2.7 | Process of the optical transition: (a) direct bandgap transition (b) indirect bandgap transition (c) impurity-band transition and (d) Intra-band transition | 24 |
| Figure 2.8 | Optical emission spectra of a single InGaAs/GaAs QD at different laser excitation levels | 41 |
| Figure 2.9 | Cross-sectional view of an ideal lens-shaped QD. (AB) = ρ_0 , (MN) = s the radius at the base, and (GN) = h the height of the dot | 49 |
| Figure 2.10 | (a) and (b) Picture of MBE system. (c) Schematic diagram of the growth chamber | 52 |
| Figure 2.11 | Overall process of fabrication semiconductor structure included measurement and data analysis | 53 |

| | | |
|-------------|---|----|
| Figure 2.12 | Schematic representation of the three important growth modes of a film: Frank van der Merwe (FM), Stranski Krastanow (SK), and Volmer Weber (VM) modes | 55 |
| Figure 2.13 | Illustration of island formation during epitaxial growth of a semiconductor material on top of another semiconductor with a smaller lattice constant in Stranski-Krastanow mode to form the QD | 56 |
| Figure 2.14 | Schematic diagram of (a) 3-D self-assembled aligned QD model and (b) the AFM images related with self-assembled aligned QD structure... | 58 |
| Figure 2.15 | The example of timeline process of (a) the superlattice template structure and (b) the InGaAs induction layer structure | 59 |
| Figure 2.16 | Schematic diagram of absorption process in semiconductor structure.... | 61 |
| Figure 2.17 | Absorption spectrum for free carriers in an electric field according to Eq. (2.65)..... | 66 |
| Figure 2.18 | Band structure of semiconductor when electric field is applied with (a) no photon and (b) the photon of energy $\hbar\omega < E_g$ | 68 |
| Figure 2.19 | In an electric field, the band edges become tilted. The wavefunctions therefore become airy-functions and penetrate into the bandgap region. This enables absorption of photons with energies below the band gap energy and to an oscillating absorption above the bandgap | 68 |
| Figure 2.20 | Illustration of the exciton resonances in QW structure, which are clearly seen in the absorption spectra even at room temperature | 69 |
| Figure 2.21 | Illustration of (a) calculated wave functions and energy levels for a 150 Å thick GaAs-like quantum well at 0 and 10^5 V/cm and (b) calculated absorption of a 150 Å thick GaAs-like quantum well at 10^5 V/cm. The individual transitions are labeled (n_v, n_c) where $n_v(n_c)$ is the valence (conduction) subband number. The smooth line is the calculated Franz-Keldysh effect for bulk material (Figure 2.17) | 73 |
| Figure 2.22 | Impact of an electric field on (a) bulk material (tilt of bands) and (b) a quantum well (QCSE) | 74 |

| | | |
|-------------|--|----|
| Figure 2.23 | Impact of electric fields on the absorption spectrum of a AlGaAs/GaAs quantum well. (a): Electric field along the [001] growth direction, (i) – (v): $E = 0, 0.6, 1.1, 1.5, \text{ and } 2 \times 10^5$ V/cm. (b): Electric field within the interface plane, (i, ii, iii): $E = 0, 1.1, \text{ and } 2 \times 10^5$ V/cm | 75 |
| Figure 2.24 | Schematic diagram of the QW structure when (a) no applied electric field and (b) the electric field is applied in perpendicular to the layers ... | 76 |
| Figure 2.25 | Schematic diagram of the absorption spectra versus energy in the presence of applied electric field on QW structure. The decreasing and broadening of absorption peak is larger when electric field is increased, consistency with the results of both theoretically and experimentally..... | 78 |
| Figure 2.26 | Schematic diagram of a confined exciton in a QD of a radius R under the uniform applied electric field \vec{E}_a . ϵ_d and ϵ_g are the dielectric constants of the QD and the glass matrix, respectively. The z axis is along the direction opposite to the applied electric field \vec{E}_a . \vec{E}_d is the electric field inside the QD | 81 |
| Figure 2.27 | Illustration of (a) the energy levels of exciton as a functions of applied electric field in a CdS QD of radius R , (b) energy shifts of the ground state exciton as a functions of applied electric field for QD sizes of $R = 9$ nm (solid line) and $R = 5$ nm (dotted line), (c) energy shifts of the ground state (solid line) and the first (dotted line) and the second (dashed line) of the confined exciton as a functions of QD size with electric field 1.25×10^4 V/cm, and (d) energy shifts of the ground state exciton in QD as a functions of R for two representative electric field 5×10^4 (dotted line) and 1.5×10^5 (solid line) | 84 |
| Figure 2.28 | Representation of (a) electron and hole distribution functions in the absence of an applied electric field in QD for three different sizes of $R = 2$ nm (solid line), 5 nm (dotted line) and $R = 8$ nm (dashed line) in the absence of electric field, (b) in the presence of an applied electric field 1.5×10^5 V/cm..... | 87 |

| | | |
|-------------|---|----|
| Figure 2.29 | The electron (a) and hole (b) distribution functions in QD for three different magnitudes of $E = 0$ (solid line), 10^5 V/cm (dotted line), and 2×10^5 V/cm (dashed line) with $R = 9$ nm | 88 |
| Figure 2.30 | The induced electric dipole moment as a function of applied electric field for a QD of size $R = 9$ nm..... | 89 |
| Figure 2.31 | The relative decay rate of exciton as a function of the applied electric field for the ground state exciton in QD of size $R = 9$ nm (solid line), 5 nm (dotted line) | 90 |
| Figure 2.32 | The ground state energy level (solid lines) and the first excited state energy level (dotted lines) of electron as a function of electric fields along the growth direction (a) and along the parallel direction (b) with the diameter and height of the QD are 10 and 3 nm, respectively. The first four energy levels of the hole as functions of electric fields along the growth direction (c) and along the parallel direction (d) with the same diameter of the QD. The solid lines, dotted lines, dashed lines, and short-dashed lines in (c) and (d) correspond to the first heavy-hole, the first light-hole, the second heavy-hole, and the third heavyhole energy levels, respectively | 93 |
| Figure 2.33 | The transition energies of the first electron energy level to the first heavy-hole energy level along the growth direction. The diameter and height of the QD are 5 nm. The black circles are experimental results.... | 94 |
| Figure 2.34 | Schematic of sample structure (a) and the AFM image of the reference sample (b). The quantum dots exhibit bimodal size distributions. QD1 and QD2 are assigned to denote the small and the large quantum dots, respectively | 96 |

| | | |
|-------------|---|-----|
| Figure 2.35 | The ER spectrum in the photon energy range of 1.24–2.4 eV of the investigated sample under zero bias voltage at 77 K. Integers are FKO extremum indices. The bias voltage dependence of the built-in electric field in the undoped GaAs layer is presented in the inset by closed squares. The solid line is intended as visual guides..... | 97 |
| Figure 2.36 | The ER spectra for QD1 under various bias voltages at 77 K (shifted vertically for clarity). The dashed line is a guide for the eyes | 98 |
| Figure 2.37 | The electric field dependence of the ground-state interband transition energy of QD1. The solid parabola is a least-squares fit to Eq. (2.88). When the electric field is 43.0 kV/cm, the parabola reaches its top..... | 99 |
| Figure 2.38 | Different polarization states of laser emission, illustrated for a few cycle pulse propagating from left to right | 103 |
| Figure 2.39 | Schematic illustrations and SEM images of (a) a wall-shaped structure and (b) an air bridge, both with a length of 10 nm and a width of 400 nm. The thickness of the air bridge is 50 nm. (c) Polarization degrees in wall-shaped structure (solid squares) and air bridges (open circles). The ratios of the polarization degree in the wall-shaped structure to that in the air bridge, measured at the same positions, are shown by triangles..... | 106 |
| Figure 2.40 | Illustration of degree of linear polarization of interband transitions (a), and (b) polarization of envelope functions of p_x and p_y orbitals calculated as a function of aspect ratio. The probability density of a valence-band electron occupying the p_x orbital (a) and p_y orbital (b) and schematic distribution of p_x (c) and p_y (d). (g) plots an optical anisotropy calculated as a function the height of the QDs | 107 |

| | | |
|-------------|---|-----|
| Figure 2.41 | (a) For an InAs/GaAs self-assembled QD elongated along the $[1\bar{1}0]$ direction, the intensity of the emission, respectively, polarized along the $[1\bar{1}0]$ (thin lines) and $[110]$ (thick lines) directions calculated for single exciton, biexciton, and triexciton. (b) For a non-interacting electron-hole pair, single exciton, biexciton and triexciton, the calculated linear polarization as a function of the aspect ratio of the QD. Inset: a schematic view of an elongated QD | 110 |
| Figure 2.42 | Thin quantum dot considered in theoretical calculation. The electric field is applied along the x direction. An electron and a hole are confined in the quantum dot by an infinitely high confinement potential..... | 113 |
| Figure 2.43 | Calculated hole wave functions for a $L_x = L_y = 30$ nm QD. Wave functions as a function of the (a) y position, and (b) x position. In (a), the wavefunctions are plotted for the y position with the x position set at the maximum wave function. In (b), the y position is fixed at 15 nm, which is the center of the QD..... | 114 |
| Figure 2.44 | Effective dot sizes plotted as functions of the electric field. They are obtained from calculated wave functions by fitting them to sinusoidal functions | 115 |
| Figure 2.45 | (a) Electric-field dependence of the calculated degree of polarization. The degree of polarization has a positive value for polarized optical emission and absorption in the y direction. (b) Calculated wave functions of electrons and holes for quantum dots with different lateral sizes. The electric field is 30 kV/cm | 117 |

| | | |
|-------------|--|-----|
| Figure 2.46 | (a) Schematic diagram of the sample used in the measurement. Two quantum dots positioned centrally between the electrodes were detected in the measurement. (b) Polarization resolved PL with application of the electric field for the larger dot. 0° means that the PL polarization is parallel to the electric field. R represents the PL ratios between 0 and 4 V. The excitation intensity is 2 mW, which is under a low excitation condition. (c) Polarization resolved PL with application of the electric field for the smaller dot | 119 |
| Figure 3.1 | Schematic diagram of InAs/GaAs linearly aligned quantum dots shown by AFM image (top view). (b) The mathematical model corresponding to AFM image and (c) band diagram related with | 123 |
| Figure 3.2 | Illustration of (a) finite-difference approximation by different geometric interpretations of the first-order finite difference approximation related to forward, backward, and central difference approximation. (b) Simple diagram of reduction from high order derivatives to lower order derivatives | 126 |
| Figure 3.3 | The discretized mesh points for the two-dimensional Schrödinger equation | 127 |
| Figure 3.4 | Illustration of the band gaps in the QD material InAs and the embedding material GaAs with ratio between ΔE_c and ΔE_v is 0.7 : 0.3..... | 129 |
| Figure 3.5 | Schematic diagram of coupling behavior of four coupled QDs with dot separation (a) 6 nm, (b) 2 nm, and (c) 0 nm (calculated by Matlab®)..... | 131 |
| Figure 3.6 | Schematic diagram of coupling behavior of four coupled QDs with dot separation (a) 6 nm, (b) 2 nm, and (c) 0 nm (calculated by COMSOL)..... | 133 |
| Figure 3.7 | The ground-state electron wavefunction of (a) isotropic single QD whose size is $12 \times 12 \text{ nm}^2$ and (b) elongated QD (in x direction) with size of $12 \times 108 \text{ nm}^2$ | 137 |
| Figure 3.8 | The polarization degree of single QD whose size in the x direction was elongated from 12 to 144 nm while that in the y direction was maintained at 12 nm..... | 138 |
| Figure 3.9 | The polarization degree of elongated QDs with different aspect ratio of (a) 2, (b) 3, (c) 4, and (d) 5, respectively | 139 |

| | | |
|-------------|---|-----|
| Figure 3.10 | Bar chart for PD values of QDs with various sizes and aspect ratios | 140 |
| Figure 3.11 | Schematic diagram of two-dimensional aligned QD system. Each QD size is $n \times a \text{ nm}^2$ and interdot spacing $d \text{ nm}$ | 141 |
| Figure 3.12 | The ground-state electron wavefunction of twelve QDs (highest number of QDs that can be calculated), each of size $12 \times 12 \text{ nm}^2$ with interdot spacing of 12 nm | 143 |
| Figure 3.13 | Comparison of overlap integral (pink line), RawPD (red line), and total PD (blue line) vs. the number of QDs aligned in the x direction. The dot size was maintained at $12 \times 12 \text{ nm}^2$ (isotropic shape), and the interdot spacing between adjacent QDs was fixed at 2 nm . The number of QDs increased in the x direction. The PD of elongated single QD (violet line) was also plotted for comparison..... | 144 |
| Figure 3.14 | The ground-state electron wavefunction of binary QDs, each of size $12 \times 12 \text{ nm}^2$ with interdot spacing of 22 nm | 145 |
| Figure 3.15 | (a) The polarization degree of 2, 4 and 6 QDs, and (b) the overlap integral of aligned QDs vs. their interdot spacing (dot size was fixed at $12 \times 12 \text{ nm}^2$ and the interdot spacing was varied from 0 to 18 nm)..... | 146 |
| Figure 3.16 | (a) The polarization degree of two isotropic QDs, and (b) the overlap integral of aligned QDs with various dot sizes varied from $12 \times 12 \text{ nm}^2$ to $48 \times 48 \text{ nm}^2$. The interdot spacing was also plotted at 2, 6, and 10 nm , respectively | 148 |
| Figure 3.17 | (a) The polarization degree of two isotropic QDs, and (b) the overlap integral of aligned QDs with various dot sizes varied from $12 \times 12 \text{ nm}^2$ to $40 \times 40 \text{ nm}^2$. The interdot spacing was also plotted at 2, 6, and 10 nm , respectively | 149 |
| Figure 3.18 | Schematic diagram of (a) self-aligned QD structure and (b) the configuration of two-dimensional electric field system | 152 |
| Figure 3.19 | Geometry of a rectangular grid used to approximate a 2D electrostatics problem, and (b) expansion view of the “computational molecule” used to solve the finite difference problem | 154 |

| | | |
|-------------|--|-----|
| Figure 3.20 | Schematic diagram of linearly matrix equation of potential $\Phi(x,y)$ which stand for all free nodes in the two-dimensional potential system. The specification matrix (matrix A) shows a sparse matrix with diagonal form..... | 158 |
| Figure 3.21 | Schematic diagram of (a) 6×6 two-dimensional potential system composed of the dimension of free nodes with the dimension of 4×4 and the applied voltage along both x and y direction. (b) The linearly matrix equation corresponding to the system, in form of $AX = B$. The matrix A is a square matrix, corresponding to the square of free nodes 's dimension..... | 159 |
| Figure 3.22 | illustration of 5×5 two-dimensional potential system. The electric field is applied along x direction. The interface between two materials is considered at Φ_{12} , Φ_{22} , and Φ_{32} (green frame)..... | 162 |
| Figure 3.23 | Comparison of the formula between potential element and electric field element. The potential $\Phi(x,y)$ was obtained from four surrounding nodes, but the electric field was obtained from two adjacent node in the horizontal line for E_x and vertical line for E_y | 164 |
| Figure 3.24 | Schematic diagram of (a) 6×6 two-dimensional potential system of material a with dielectric constant ϵ_1 embedded in the larger material with dielectric constant ϵ_2 . The voltages are applied at top and right edge of potential system. (b) The linearly matrix equation corresponding to the system, in form of $AX = B$ | 165 |
| Figure 3.25 | Three-dimensional contour of potential distribution of two QDs embedded in GaAs capping layer corresponding to the two-dimensional system by Matlab® programming | 168 |
| Figure 3.26 | Comparison of two-dimensional potential distribution between (a) Matlab® and (b) COMSOL programming in case of voltage was applied only in the x direction with the magnitude of 10 V. (c) Three-dimensional contour of potential distribution and (d) distribution of electric field's direction represented as the red arrows with normalized magnitude..... | 171 |

- Figure 3.27 Comparison of two-dimensional potential distribution between (a) Matlab® and (b) COMSOL programming in case of voltage was applied only in the y direction with the magnitude of 10 V. (c) Three-dimensional contour of potential distribution and (d) distribution of electric field's direction represented as the red arrows with normalized magnitude..... 173
- Figure 3.28 Comparison of two-dimensional potential distribution between (a) Matlab® and (b) COMSOL programming in case of voltage was applied both x and y direction with the magnitude of 10 and 5 V, respectively. (c) Three-dimensional contour of potential distribution and (d) distribution of electric field's direction represented as the red arrows with normalized magnitude..... 175
- Figure 4.1 (a) The normalized conduction band (CB) structure (left) and valence band (VB) structure (right) of elongated QD whose size is 24x48 nm². (b)The ground-state electron (left) and hole (right) wavefunctions related to CB and VB, respectively. (c) The normalized conduction band (CB) structure (left) and valence band (VB) structure (right) of binary QDs, each of size 12x12 nm² with interdot spacing of 2 nm. (d)The ground-state electron (left) and hole (right) wavefunctions related to CB and VB, respectively. These results are under the condition of no electric field in any directions (E_x and $E_y = 0$ V/nm)..... 184

- Figure 4.2 (a) The normalized conduction band (CB) structure (left) and valence band (VB) structure (right) of elongated QD whose size is $24 \times 48 \text{ nm}^2$. The results are for applied voltage with a magnitude of 0.008 V parallel to the x direction or direction of QD elongation (producing an electric field in the same direction ($E_x > 0, E_y = 0 \text{ V/nm}$)). (b) The ground-state electron (left) and hole (right) wavefunctions related to CB and VB, respectively. (c) The normalized conduction band (CB) structure (left) and valence band (VB) structure (right) when the elongated QD is the under the applied voltage with a magnitude of 0.008 V parallel to the y direction or perpendicular direction ($E_y > 0, E_x = 0 \text{ V/nm}$). (d) The ground-state electron (left) and hole (right) wavefunctions for CB and VB, respectively 186
- Figure 4.3 (a) The normalized conduction band (CB) structure (left) and valence band (VB) structure (right) of binary QDs, each of size $12 \times 12 \text{ nm}^2$ with interdot spacing of 2 nm . The results are under the applied voltage with a magnitude of 0.008 V parallel to the x direction or aligned QD direction (producing an electric field in the same direction ($E_x > 0, E_y = 0 \text{ V/nm}$)). (b) The ground-state electron (left) and hole (right) wavefunctions related to CB and VB, respectively. (c) The normalized conduction band (CB) structure (left) and valence band (VB) structure (right) when the binary QDs is the under the applied voltage with a magnitude of 0.008 V parallel to the y direction ($E_y > 0, E_x = 0 \text{ V/nm}$). (d) The ground-state electron (left) and hole (right) wavefunctions for CB and VB, respectively 188
- Figure 4.4 The polarization degree of elongated QD ($24 \times 48 \text{ nm}^2$), binary QDs, and four QDs ($12 \times 12 \text{ nm}^2$) under the applied voltage in the (a) x direction (parallel to the alignment of QD) and (b) y direction (normal to the alignment of QD) with the range between 0.001 and 0.005 V 189
- Figure 4.5 Diagram of investigation of linear polarization degree on single and aligned QD structure in presence of an applied electric field 190

| | | |
|-------------|---|-----|
| Figure 4.6 | (a) The polarization degree of single QD with an isotropic shape ($48 \times 48 \text{ nm}^2$) vs. applied voltage V_x varied from 0 to 0.005 V. (b) The ground-state hole wavefunction under the V_x of 0, 0.001, 0.003, and 0.005 V, respectively | 192 |
| Figure 4.7 | (a) The PD of single QD under the applied voltage V_x chosen of 4 values (0.001, 0.003, 0.005, and 0.007 V) vs. the increase of QD size in the x direction elongated from 12 to 144 nm. (b) The ground-state hole wave-function of $12 \times 120 \text{ nm}^2$ QD under V_x of 0, 0.002, and 0.005 V, respectively | 195 |
| Figure 4.8 | The polarization degree of single QDs vs. applied voltage V_x (varied from 0 to 0.005 V) with the aspect ratio of (a) 1, (b) 2, (c) 3, and (d) 4, respectively | 200 |
| Figure 4.9 | Manhattan bar chart for PD values of QDs with various sizes and aspect ratios under the applied voltage of (a), 0 (zero field) (b), 0.002 (c), 0.004 and (d) 0.008 V, respectively..... | 202 |
| Figure 4.10 | The polarization degree vs. the number of $12 \times 12 \text{ nm}^2$ QDs with their spacing of 2 nm under the applied voltage fixed at 0.001, 0.005, and 0.01 V, respectively | 207 |
| Figure 4.11 | (a) The polarization degree of 2, 4, and 6 QDs and the stacked bar chart of RawPD and overlap integral (x100%) values corresponding to (b) 2, (c) 4, and (d) 6 dots, respectively under the applied voltage varied from 0 to 0.05 V. The QDs size and distance between them are the same as Figure 4.10..... | 210 |
| Figure 4.12 | (a) The PD values (left perpendicular axis) and overlap integral (right perpendicular axis) of 8, 10, and 12 QDs under the applied voltage varied from 0 to 0.003 V. The QDs size and distance between them are the same as Figure 4.10..... | 214 |
| Figure 4.13 | The polarization degree of $12 \times 12 \text{ nm}^2$ QDs vs. the number of QDs at three different interdot spacing of 2, 6, and 10 nm respectively under two constant applied voltages of (a) 0.001 V and (b) 0.005 V..... | 218 |

- Figure 4.14 The polarization degree of $12 \times 12 \text{ nm}^2$ (a1) 2, (a2) 4, and (a3) 6 QDs vs. applied voltage varied from 0 to 0.005 V at four different interdot spacing of 2, 6, 10, and 18 nm respectively. The overlap integral and RawPD corresponding to PD values of (a2 & a3) 2, (b2 & b3) 4, and (c2 & c3) 6 QDs, respectively..... 225
- Figure 4.15 The polarization degree vs. the number of QDs at three different QD sizes of 12×12 , 16×16 , and $20 \times 20 \text{ nm}^2$ respectively under two constant applied voltages of (a) 0.001 V and (b) 0.005 V. An interdot spacing was fixed to 2 nm..... 227
- Figure 4.16 The polarization degree vs. applied voltage of five different QDs sizes: 12×12 , 16×16 , 20×20 , 40×40 , and $56 \times 56 \text{ nm}^2$, respectively (for 4 QDs case, the QDs sizes of 40×40 , and $56 \times 56 \text{ nm}^2$ were replaced by 28×28 , and $40 \times 40 \text{ nm}$, respectively, and for 6-QDs case, there were three different QD sizes: 12×12 , 20×20 , and $24 \times 24 \text{ nm}^2$) at two conditions of interdot spacing: 2 nm corresponding to applied voltage varied from 0 to 0.005 V of 2 (a1), 4 (b1), and 6 (c1) QDs, respectively, and 6 nm corresponding to applied voltage varied from 0 to 0.0005 V of 2 (a2), 4 (b2), and 6 (c2) QDs, respectively..... 232
- Figure 4.17 The $V_{PD(\max)}$ vs. QDs sizes of 12×12 , 16×16 , 20×20 , 24×24 , 28×28 , and $40 \times 40 \text{ nm}^2$ with three different numbers of QDs: 2, 4, and 6 QDs at interdot spacing of (a) 2 nm, and (c) 6 nm, respectively. The $V_{PD(\max)}$ vs. number of QDs (2, 4, and 6 QDs) with 6 QD sizes mentioned above at interdot spacing of (b) 2 nm, and (d) 6 nm, respectively..... 232
- Figure 4.18 (a) Comparison of polarization degree (in form of table) of 4 different cases: QDs size, spacing between QDs, number of QDs, and electric field strength of aligned QDs (the highlight rectangular represents an adjusted parameter in each case). (b) The pie chart of PD results 237